CRREL REPORT 90-8

DTIC FILE COPY
AD-A230 180

(12) CRREL

# Estimates of Shock Wave Attenuation in Snow

Jerome B. Johnson

October 1990

DTIC
ELECTE
DEC 20 1990
S D
D

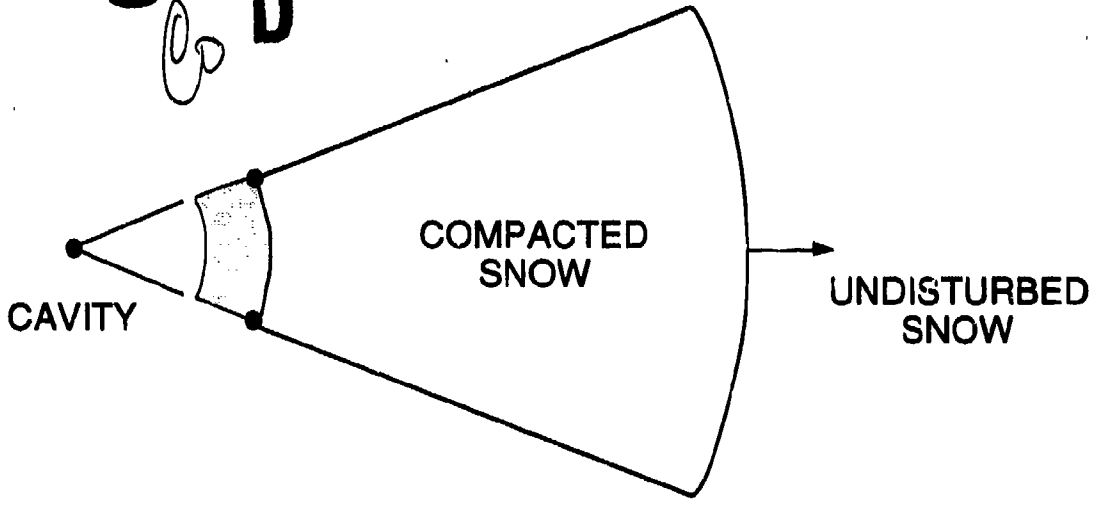


DISTRIBUTION STATEMENT A
Approved for public release;
Distribution Unlimited

90 12 20 182

*For conversion of SI metric units to U.S./British customary units of measurement consult ASTM Standard E380,* Metric Practice Guide, *published by the American Society for Testing and Materials, 1916 Race St., Philadelphia, Pa. 19103.*

*Cover: Deformation geometry for diverging shock waves (shaded area within cavity is the distance the snow surface has moved).*

CRREL Report 90-8

**U.S. Army Corps of Engineers**
Cold Regions Research & Engineering Laboratory

# Estimates of Shock Wave Attenuation in Snow

Jerome B. Johnson

October 1990


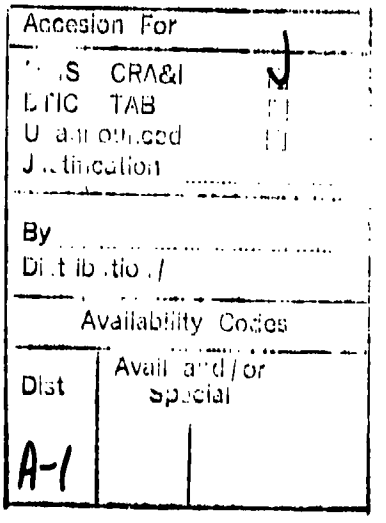


Prepared for
OFFICE OF THE CHIEF OF ENGINEERS

Approved for public release; distribution is unlimited.

## PREFACE

This report was prepared by Dr. Jerome B. Johnson, Geophysicist, Applied Research Branch, Experimental Engineering Division, U.S. Army Cold Regions Research and Engineering Laboratory. The research described in this report was funded by DA Project 4A762784AT42, *Cold Regions Engineering Technology;* Work Unit CS/012, *Attenuation of Shock Waves by Snow.*

Dr. J.A. Brown (Los Alamos National Laboratory), Dr. E.S. Gaffney (Ktech Corp.) and K. Jones (CRREL) technically reviewed this report.

The contents of this report are not to be used for advertising or promotional purposes. Citation of brand names does not constitute an official endorsement or approval of the use of such commercial products.

## CONTENTS



## ILLUSTRATIONS



## TABLE

## NOMENCLATURE

| | |
|---|---|
| $a$ | time at which the applied pressure impulse ends |
| $a_i$ | times that define the constant pressure square wave segments |
| $A_i$ | $\left[V_{i-1}^2(X_{a_i}) - \gamma b_i\right] X_{a_i}^2$ |
| $b_i$ | weighting coefficients determined from $f(t)$ |
| $B_i$ | $\gamma b_i$ |
| $D$ | shock wave propagation speed |
| $d_{LC}$ | shock penetration depth in a deep snow cover |
| $f(t)$ | function describing the shape of a variable pressure impulse |
| $H, dH$ | momentum per unit area and its derivative |
| $H_p$ | total momentum per unit area applied to the snow |
| $H_{p_i}$ | momentum per unit area applied to the snow in the $i$th square wave segment |
| $H_s$ | momentum per unit area in the snow |
| $I_0$ | instantaneously applied pressure impulse |
| $m, dm$ | mass per unit area and its derivative |
| $P$ | shock wave pressure |
| $P_0$ | maximum pressure amplitude of the shock |
| $P(t)$ | shock pressure amplitude as a function of time |
| $r$ | current position of the inner radius of the cavity surface |
| $R$ | shock wave propagation radius |
| $R_0$ | initial radius of a cavity surface in the snow |
| $t, dt$ | time and its derivative |
| $t_f$ | time required for the shock to reach $X_f$ |
| $t_0$ | time at which the pressure impulse is applied |
| $U_0$ | distance snow surface has moved |
| $V$ | snow particle velocity |
| $V_i$ | snow particle velocity in the $i$th square wave segment |
| $X_a$ | shock front position at $t = a$ |
| $X_{a_i}$ | shock front position at $t = a_i$ |
| $X_f$ | shock front position; $X_f = X_f - X_0$ for $X_0 = 0$ |
| $X_i$ | current snow surface position |
| $X_0$ | initial snow surface position |
| $\alpha$ | attenuation coefficient |
| $\beta$ | relative snow compaction $(1 - \rho_0/\rho_f)$ |
| $\gamma$ | $P_0\beta/P_f(1-\beta)$ |
| $\varepsilon$ | $R - R_0$ |
| $\rho_f$ | compacted snow density |
| $\rho_0$ | initial snow density |

# Estimates of Shock Wave Attenuation in Snow

JEROME B. JOHNSON

## INTRODUCTION

Shock wave attenuation in snow is affected by the amplitude, geometry and duration of a shock, as well as the mechanical properties of the snow. Accordingly, these effects must be taken into account in any description of shock attenuation. The mechanical properties of snow for high-strain-rate, large-amplitude shocks are not now well understood. Consequently, attempts to estimate shock attenuation in snow have relied on field measurements of pressure attenuation from explosions in snow and on theoretical constitutive descriptions.

Mellor (1977) used the results from field measurements of explosive detonations in snow to estimate the attenuating properties of snow for spherical shock waves. He estimated that the attenuation of shock pressure, combining geometric spreading and internal dissipation, near an explosion decays as $R^{-4}$ ($R$ being the propagation radius) and close to the elastic limit it is approximately an $R^{-3}$ decay. Brown (1980, 1981, 1983) appears to have made the first and only attempts to estimate shock attenuation for plane waves in snow. He used two theoretical volumetric constitutive laws, one for medium to high density snow and one for low density snow, to estimate shock attenuation. His results indicate that plane shock waves can attenuate by more than 80 to 90% after propagating through only 0.04 to 0.06 m of snow. These are large attenuations that are, at their maximum, about an $(X_f - X_0)^{-1.2}$ decay ($[X_f - X_0]$ is the propagation distance).

Brown did not discuss the importance of an applied shock's amplitude, geometry and duration on attenuation features. This paper will examine the importance of the pressure–time profile of an applied pressure impulse on shock attenuation in snow. Snow will be represented by a simple mechanical model in which attenuation occurs through momentum transfer from the applied shock to the snow.

## MOMENTUM MODEL

The momentum model, also known as the "snowplow" model, was used in initial attempts at developing constitutive relations to analyze the dynamic behavior of porous materials (Herrmann 1971). The porous material is assumed to compact to its final density at a negligible stress. After compaction, the material is assumed to be incompressible (an ideal locking material). The change in momentum caused by a stress wave (the pressure impulse) is assumed to be spread uniformly over the volume of the material behind an advancing shock wave. This means that the stress wave is lengthened in time and reduced in amplitude as more of the material is compacted by the propagating shock. Hence, attenuation is caused by momentum spreading, and losses attributable to plastic deformation, fracturing and release waves are not considered.

## INSTANTANEOUSLY APPLIED IMPULSE

Consider a pressure impulse ($I_0$) applied normal to the plane surface of snow, and assume that snow is an ideal locking material. Snow next to the surface will be immediately compacted to its final density. Since the compacted snow is rigid, it will move at a uniform pressure and particle velocity after the pressure impulse is applied. The stress wave will propagate into the snow as a compaction shock, moving with a velocity $D$ at a pressure $P$ and particle velocity $V$. At the shock front these parameters are related by the Rankine–Hugoniot jump conditions for the conservation of mass and momentum across the shock front (Kolsky 1963)

$$\rho_0 D = \rho_f [D-V] \tag{1}$$

and

$$P = \rho_0 DV \tag{2}$$

where $\rho_0$ is the initial density of the snow and $\rho_f$ is the compacted snow density. The compacted snow density $\rho_f$ is usually determined by experiment, but is estimated for this paper because of the lack of suitable data. In using eq 1 and 2, the contribution of shock heating in the snow is neglected.

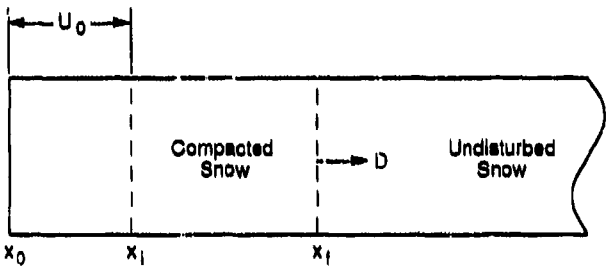


*Figure 1. Deformation geometry for plane shock wave propagation in snow.*

Figure 1 shows the deformation geometry in one dimension for a pressure impulse applied at the initial snow surface $X_0$. The location of the surface of the snow and the shock front at some time after the application of the pressure impulse are $X_i$ and $X_f$ respectively. During the time that the shock front has traveled to $X_f$, the snow surface has moved a distance $U_0$. $U_0$ is a function of time or, alternatively, a function of shock propagation position $X_f$. At any time the location of the snow surface is

$$X_i = X_0 + U_0. \tag{3}$$

The displacement of the snow surface can be calculated by integrating the particle velocity over time

$$U_0 = \int_{t_0}^{t_f} V\, dt \tag{4}$$

where $t_0$ is the time that the shock is applied and $t_f$ denotes the time required for the

shock to reach $X_f$. Knowing the shock pressure attenuation with distance is of more practical interest than following the pressure with time. Thus, the snow surface displacement will be reformulated in terms of shock position rather than time. By use of the fact that

$$D = \frac{dx}{dt} \tag{5}$$

eq 4 may be rewritten as

$$U_0 = \int_{X_0}^{X_f} \frac{V}{D}\, dx\,. \tag{6}$$

From eq 1

$$\frac{V}{D} = \left(1 - \frac{\rho_0}{\rho_f}\right) = \beta \tag{7}$$

where $\beta$ describes the relative snow compaction. Substituting eq 7 into eq 6 and solving gives the position of the snow surface at time $t_f$

$$X_i = (1-\beta)\, X_0 + \beta X_f\,. \tag{8}$$

The mass and momentum per unit area of the snow per unit length contained in the length $(X_f - X_i)$ between the current snow surface position $X_i$ and shock front position $X_f$ are

$$dm = \rho_f\, dx \tag{9}$$

$$dH = \rho_f V\, dx\,. \tag{10}$$

Since the compacted snow is assumed to be rigid, $V$ is constant through the region $X_i$ to $X_f$ and is equal to the particle velocity at $X_f$, i.e. $V = V(X_f)$. Consequently, the momentum per unit area in the snow at the time the shock has reached $\rho_f$ is

$$H_s = \int_{X_i}^{X_f} \rho_f V\, dx = V \rho_f\, (X_f - X_i)\,. \tag{11}$$

Substituting in for $X_i$ from eq 8 gives

$$H_s = \rho_f V\, (1-\beta)(X_f - X_0)\,. \tag{12}$$

The momentum per unit area in the snow $H_s$ must be equal to the momentum per unit area applied to the snow from the instantaneously applied pressure impulse that is given by

$$H_p = I_0\,. \tag{13}$$

Equating $H_s$ and $H_p$ and solving for $V$ gives

$$V = \frac{I_0}{\rho_f(1-\beta)(X_f - X_0)}. \tag{14}$$

Equations 7 and 14 can be used in eq 2 to determine the pressure at the shock front

$$P(X_f) = \frac{\rho_0 V^2}{\beta} = \frac{I_0^2}{\rho_0 \beta (X_f - X_0)^2}. \tag{15}$$

Figure 2 shows the shock front pressure for snow subjected to an instantaneous pressure impulse of $I_0 = 100$ Pa s. The pressure attenuates as $(X_f - X_0)^2$, with proportionality constants that depend on impulse magnitude, initial snow density and the relative snow compaction $\beta$. Figure 2a shows that snow with a higher initial density supports less pressure at the same propagation distance as compared to lower density snow.

Equation 15 can be rewritten to show shock pressure as a function of the total mass of compacted snow

$$P(X_f) = \frac{I_0^2 \rho_0}{\beta m^2} \tag{15a}$$

where

$$m = \rho_0(X_f - X_0). \tag{15b}$$

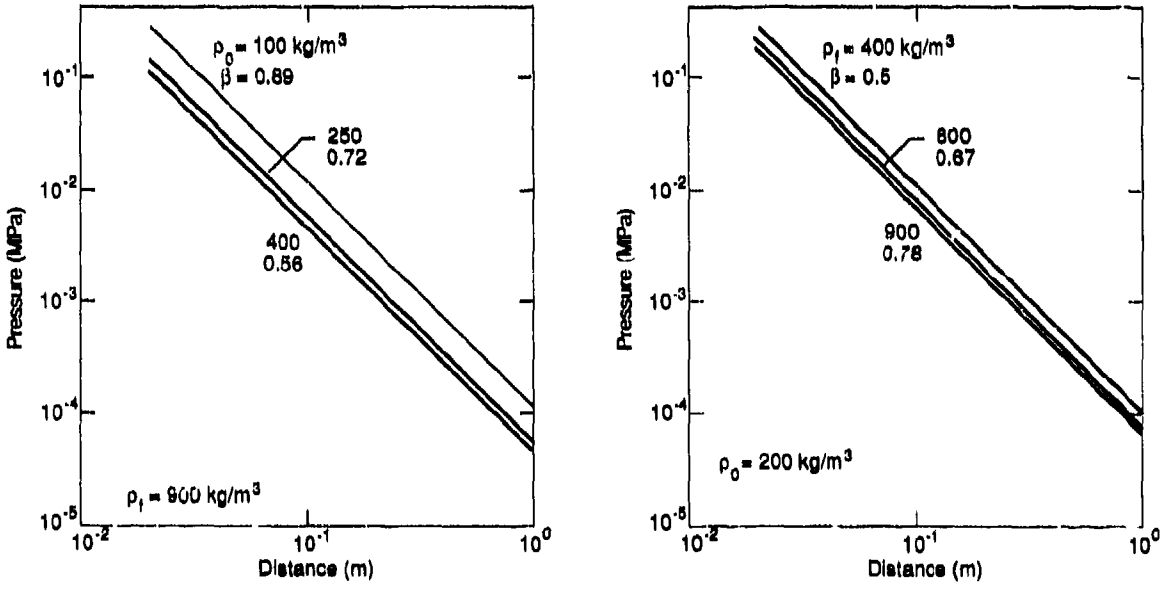


*a. Initial densities of 100, 250 and 400 kg/m$^3$ and final density of 900 kg/m$^3$.*

*b. Initial density of 200 kg/m$^3$ and final densities of 400, 600 and 900 kg/m$^3$.*

*Figure 2. Pressure decay with distance for an instantaneously applied plane shock wave pressure impulse (100 Pa s), predicted by the snowplow model.*

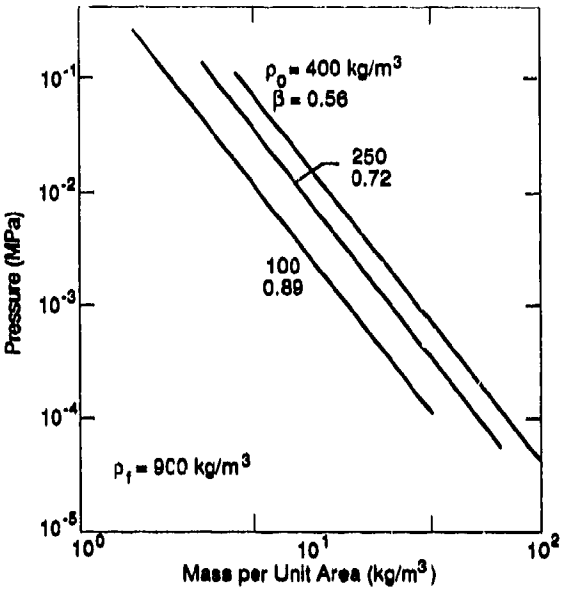


*Figure 3. Pressure decay as a function of snow mass compacted by the propagating plane shock wave, predicted by the snowplow model for the conditions given in Figure 2a.*

The results given in Figure 2a are recalculated using eq 15a and shown in Figure 3. Figure 3 shows that snow with an initially lower density will support a lower pressure magnitude than will a snow with a higher initial density, given the same total compacted mass. This finding leads to the common observation that lower density materials are better attenuators than higher density materials because less mass is needed to produce a given attenuation than for a porous material of higher density.

## CONSTANT PRESSURE IMPULSE OF FINITE DURATION

The solution given by eq 15 is not a very satisfying way of evaluating shock attenuation since it assumes instantaneous application of the pressure impulse. This is unrealistic, as it implies infinite pressure at $x = X_0$, and does not show how pressure pulses with the same total impulse but different amplitudes and durations are attenuated. An analytical solution can be derived for a constant pressure impulse of finite time duration, given by

$$\begin{aligned} P(t) &= P_0 \qquad 0 \le t \le a \\ P(t) &= 0 \qquad a < t \end{aligned} \tag{16}$$

where $a$ is the time duration of the applied pressure pulse. The momentum per unit area caused by the pressure impulse is

$$H_p = \int_0^t P_0 \, dt \qquad \text{for } 0 \le t \le a \tag{17}$$

and

$$H_p = \int_0^a P_0 \, dt \qquad \text{for } a < t \, . \tag{18}$$

Equations 17 and 18 show that the momentum during application of the pressure impulse will vary with time, while the momentum after the impulse has been applied is constant. Therefore, separate solutions for shock pressure attenuation are needed during the time period of pulse application and for the time period after the pulse has been applied. Equations 17 and 18 can be transformed into spatial coordinates by use of the results of eq 5 and 7, giving

$$H_p = \int_0^{X_f} P_0 \frac{\beta}{V} \, dx \qquad \text{for } 0 < X_f < \frac{aV}{\beta} \, . \tag{19}$$

The limits of integration are 0 to $X_a = aV/\beta$. Equating momentum in the snow (eq 12) to the pressure impulse momentum (eq 19) and differentiating gives

$$\frac{P_0 \beta}{\rho_f (1-\beta)} = V \frac{d}{dx} [V X_f] \, . \tag{20}$$

Also

$$V \frac{d}{dx} [V X_f] = \frac{1}{X_f} \frac{d}{dx} \left[ \frac{1}{2} V^2 X_f^2 \right] . \tag{21}$$

Substituting the identity in eq 21 into 20 and integrating gives the particle velocity

$$V = \left[ \frac{P_0 \beta}{\rho_f (1-\beta)} \right]^{1/2} \text{for } 0 \le X_f \le X_a \, . \tag{22}$$

Hence, during the period of pressure impulse application, the particle velocity is constant and there is no attenuation of the shock pressure. The distance that the shock has traveled at $t = a$ is given by

$$X_a = Da = \left[ \frac{P_0 a^2}{\beta \rho_f (1-\beta)} \right]^{1/2} . \tag{23}$$

After the pressure impulse momentum has been applied to the snow, the relationship between the pressure impulse momentum and snow momentum is

$$P_0 a = \rho_f V (1-\beta) X_f \qquad \text{for } X_a < X_f \, . \tag{24}$$

Solving for the particle velocity and using the definition of $X_a$ in eq 23 gives

$$V = \left[ \frac{P_0 \beta}{\rho_f (1-\beta)} \right]^{1/2} \frac{X_a}{X_f} \, . \tag{25}$$

The shock pressure as a function of distance can now be determined from eq 2, 7, 22 and 25, giving

$$P(X_f) = P_0 \quad \text{for } 0 \le X_f \le X_a \tag{26a}$$

$$P(X_f) = \frac{P_0 X_a^2}{X_f^2} \quad \text{for } X_a < X_f . \tag{26b}$$

Figure 4 (square wave) shows the pressure as a function of distance for an initial snow density of 350 kg/m$^3$, $\beta = 0.3$ and a pressure impulse of 605 Pa s. The shock does not begin attenuating until after all of the pressure impulse momentum has been applied to the snow surface, and then it attenuates as $X_f^{-2}$. Comparison of the square wave pressure impulse to an instantaneous pressure impulse (impulse) shows that the pressure is lower for the square wave during its duration of application than for an instantaneously applied pressure impulse. After the square wave momentum has been completely transferred to the snow, both the square wave and instantaneously applied impulse pressures are the same. Since explosives and other sources of shocks are applied over a finite time, this result shows the importance of modeling the pressure–time profile of an applied pressure impulse for predicting attenuation.

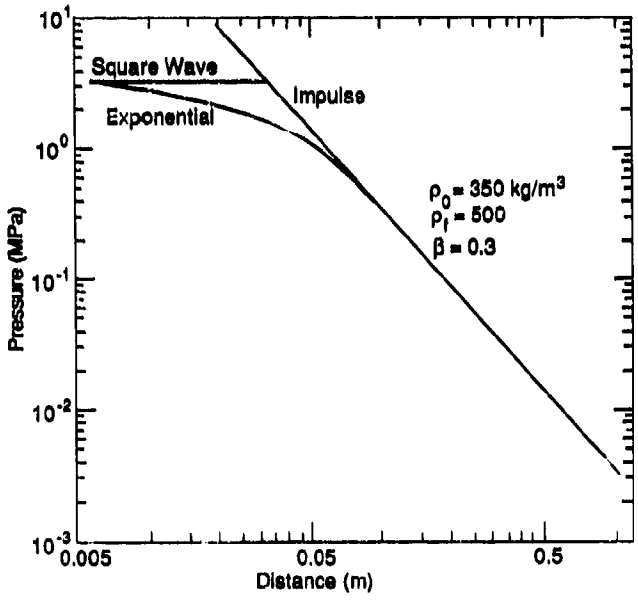


*Figure 4. Comparison of pressure decay with distance for plane shock waves, each having a total applied pressure impulse of 605 Pa s, predicted by the snowplow model. The pressure impulse was applied instantaneously for* impulse, *with a square wave of 0.17 ms duration for* square wave, *and an exponential pulse of 0.16 ms duration for* exponential.

## VARIABLE PRESSURE IMPULSE OF FINITE DURATION

Simulating a realistic applied pressure impulse requires a function that can represent variable pressure impulses of finite duration. These variable pressure impulses result in nonlinear differential equations that do not have closed form

solutions and whose numerical solutions can be unstable. In addition, the form of the differential equations depend on the particular variable pressure impulse applied to the snow surface. To reduce these computational difficulties, the variable pressure impulses were approximated by a sequence of square waves. The accuracy of such an approximation depends on the time duration specified for the square wave segments that constitute the applied pressure impulse. Thus, instead of exactly formulating the problem and obtaining a numerical solution, the pressure impulse is approximated and solved analytically within the sequential time steps. The variable pressure impulse of finite duration beginning at $t = 0$ is approximated by

$$P(t) = P_0 b_i \qquad \begin{cases} b_0 = 1 & \text{for } 0 \le t < a_1 \\ b_1 = f\left(\dfrac{a_2 + a_1}{2}\right) & \text{for } a_1 \le t < a_2 \\ \vdots & \\ b_{n-1} = f\left(\dfrac{a_n + a_{n-1}}{2}\right) & \text{for } a_{n-1} \le t < a_n \\ b_n = 0 & \text{for } a_n \le t . \end{cases} \tag{27}$$

The shape of the variable pressure impulse is $f(t)$, where the $b_i$ weighting coefficients are determined at the midpoint between the beginning time and ending time for each square wave segment $f[(a_{i+1} + a_i)/2]$. The $a_i$ are the times that define the square wave segments where $i = 1,2,3,\ldots,n-1$.

Solving for the pressure in snow as a function of distance, using eq 27, requires that the problem be formulated for three conditions. The first is for the time, or spatial increment, of the first square wave segment. The next solution must account for the momentum that has been applied to the snow at the time, or spatial position, of interest. Finally, a solution must be found after all of the pressure impulse momentum has been applied to the snow. These conditions can be expressed as

$$\int_0^{X_f} P_0 b_0 \frac{\beta}{V_0(x)}\, dx = \rho_f V_0(X_f)(1-\beta)X_f \quad \text{for } 0 \le X_f < X_{a_1} \tag{28a}$$

$$H_{P_0} + \int_{X_{a_1}}^{X_f} P_0 b_1 \frac{\beta}{V_1(x)}\, dx = \rho_f V_1(X_f)(1-\beta)X_f \quad \text{for } X_{a_1} \le X_f < X_{a_2}$$

$$\vdots \tag{28b}$$

$$\sum_{i=0}^{n-2} H_{P_i} + \int_{X_{a_{n-1}}}^{X_f} P_0 b_{n-1} \frac{\beta}{V_{n-1}(x)}\, dx = \rho_f V_{n-1}(X_f)(1-\beta)X_f$$

$$\text{for } X_{a_{n-1}} \le X_f < X_{a_n}$$

$$\sum_{i=0}^{n-1} H_{P_i} = \rho_f V_n(X_f)(1-\beta)X_f \quad \text{for } X_{a_n} \le X_f . \tag{28c}$$

There are $n+1$ equations to solve before the complete particle velocity solution can be found. Each equation depends on the solutions of the previous segments.

Equation 28a is a constant pressure impulse, with the solution given by eq 22, 23 and 26a

$$X_{a_1}^2 = \gamma \frac{a_1^2}{\beta^2} \tag{29}$$

$$V_0^2(X_f) = \gamma \quad \text{for } 0 \le X_f < X_{a_1} \tag{30}$$

where $\gamma = \dfrac{P_0 \beta}{\rho_f(1-\beta)}$ .

Equations 28b can be solved sequentially to give the solution for the spatial position of interest. These solutions can be given as a set of recursion relations for position, particle velocity, and time

$$X_{a_{i+1}}^2 = \left[a_{i+1} - a_i + \frac{\beta}{B_i}\left(A_i + B_i X_{a_i}^2\right)^{1/2}\right]^2 \frac{B_i}{\beta^2} - \frac{A_i}{B_i} \tag{31}$$

$$V_i^2(X_f) = \frac{1}{X_f^2}\left[\left(V_{i-1}^2(X_{a_i}) - \gamma b_i\right) X_{a_i}^2 + \gamma b_i X_f^2\right] \tag{32}$$

where

$$i = 1,2,\ldots,n-1 \quad \text{for } X_{a_i} \le X_f < X_{a_{i+1}}$$

and

$$A_i = \left[V_{i-1}^2(X_{a_i}) - \gamma b_i\right] X_{a_i}^2$$

$$B_i = \gamma b_i .$$

$$V_n(X_f) = \frac{\sum_{i=0}^{n-1} H_{p_i}}{\rho_f(1-\beta)\, X_f} \qquad \text{for } X_{a_n} < X_f \tag{33}$$

where

$$\sum_{i=0}^{n-1} H_{p_i} = H_p$$

is the total momentum per unit area applied to the snow. Equations 29 and 30 are used to start the solution and the recursion relations are used to follow the progression of the shock.

Figure 4 (exponential) shows the results of using eq 29 through 33, 2 and 7 to calculate the pressure as a function of shock wave propagation distance for an exponentially decaying pressure impulse (total pressure impulse = 605 Pa s)

$$P = P_0 e^{-\alpha t} \tag{34}$$

where $\alpha$ is a decay constant and $P_0$ is the initial pressure and $f(t) = e^{-\alpha t}$. Comparison

of the three different applied pressure impulses (each with the same total momentum) in Figure 4 shows that shock attenuation can be markedly different during the period of pressure impulse application. The instantaneously applied pressure impulse applies all of its momentum at once resulting in infinite initial pressure that immediately begins attenuating as $X_f^{-2}$, where $X_0 = 0$. The square wave maintains a constant pressure equal to the applied pressure until all of its momentum has been transferred to the snow and then begins to attenuate. Finally, the exponential pulse gradually attenuates while its momentum is being transferred to the snow, asymptotically approaching an $X_f^{-2}$ decay. Once a pressure impulse has been applied to the snow, pressure attenuation is controlled by the mechanical properties of the snow and the magnitude of total pressure impulse.

## ATTENUATION OF CYLINDRICAL AND SPHERICAL GEOMETRY SHOCK WAVES

Geometric spreading can greatly increase shock attenuation in snow. Torvik (1971) developed equations describing pressure decay for cylindrical and spherical geometry shock waves using the snowplow model and assuming instantaneous application of a pressure impulse. For a cylindrically spreading shock, the pressure is given by

$$P(R) = \frac{I_0^2 R_0^2 (1-\beta)^2}{\rho_0 \beta R^2 (R-r)^2} \tag{35}$$

$$r = \left[\beta R^2 + (1-\beta) R_0^2\right]^{1/2}. \tag{36}$$

The pressure for a spherically spreading shock is

$$P(R) = \frac{I_0^2 R_0^4 (1-\beta)^2}{\rho_0 \beta R^4 (R-r)^2} \tag{37}$$

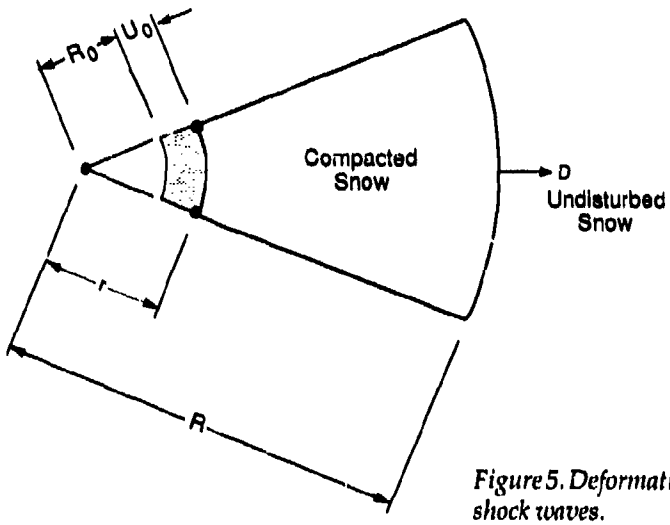


*Figure 5. Deformation geometry for diverging shock waves.*

$$r = \left[\beta R^3 + (1-\beta) R_0^3\right]^{1/3}. \tag{38}$$

$I_0$ is the instantaneously applied pressure impulse, $R_0$ is the initial radius of the cavity surface in the snow on which the pressure impulse is applied, and $r$ is the location of the inner radius of the cavity at some time after the application of the pressure impulse (Fig. 5).

When $R = R_0 + \varepsilon$, where $\varepsilon << R_0$, a cylindrical geometry shock decays as $\varepsilon^{-2}$, increasing to a decay of $R^{-4}$ for $\varepsilon >> R_0$ (Fig. 6a). A spherical geometry shock decays

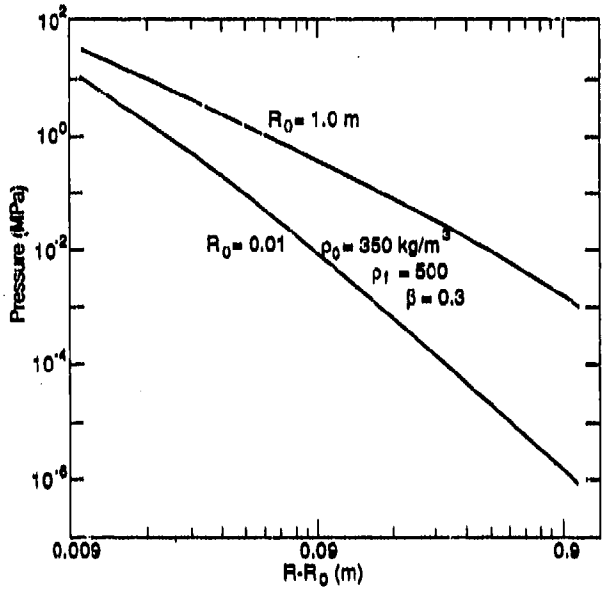


*a. Cylindrical shock waves with initial radii of 0.01 and 1.0 m, predicted by the snowplow model.*

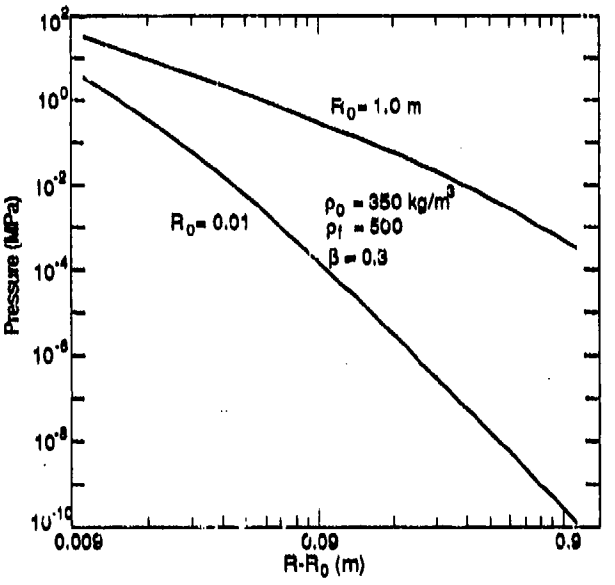


*b. Spherical shock waves with initial radii of 0.01 and 1.0 m predicted by the snowplow model.*

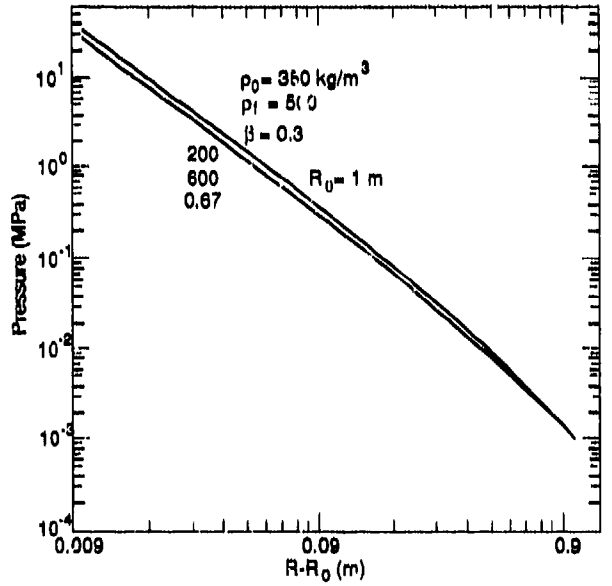


*c. Cylindrical shock waves in snow with initial densities of 200 and 350 kg/m$^3$ and initial radii of 1 m.*

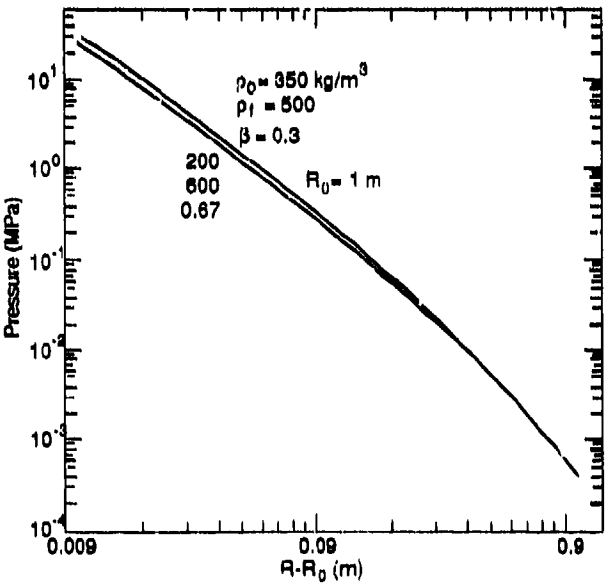


*d. Spherical shock waves in snow with initial densities of 200 and 350 kg/m$^3$ and initial radii of 1 m.*

*Figure 6. Comparison of pressure decay with distance.*

as $\varepsilon^{-2}$ for $\varepsilon << R_0$, increasing to $R^{-6}$ for $\varepsilon >> R_0$ (Fig. 6b). These findings show that pressure decay, including the effects of geometric spreading, vary significantly depending on the initial radius over which the pressure impulse is applied and the distance from the initial radius. Figures 6c and d show the effect of changes in initial snow density and $\beta$ on pressure attenuation for cylindrical and spherical waves.

## PRESSURE DECAY OF A LINE CHARGE ON SNOW

Line charges are used to clear minefields and to remove snow cornices from mountain ridge tops. Therefore, it is of practical interest to know the extent that snow reduces the effectiveness of line charge detonations. For a line charge resting on or above a snow cover, the cylindrical pressure wave that hits the snow surface has propagated primarily through the air.

Ford (1986) has measured air-blast pressure, positive phase duration and total pressure impulse at the ground as a function of lateral distance from the axis of a line charge explosion (Table 1). The positive phase duration is defined as the duration of the compressive (positive) shock pressure. Although air-blast pressures over snow would differ, it is assumed, for this example, that the air-blast pressures given in Table 1 would also occur over snow. Furthermore, the snow is assumed to be deep and shock pressures are determined only for small propagation depths into the snow so that $\varepsilon << R_0$, where $R_0$ is the distance from the line charge to the point of interest on the snow surface. With these conditions, the snow–ground boundary can be neglected and shock pressure in the snow can be estimated from the equations for a one-dimensional variable pressure impulse of finite duration (eq 29–33, 2 and 7) and an exponentially decaying pressure pulse (eq 34). Figure 7 shows the shock pressure as a function of distance from the line charge $d_{LC}$ at the snow surface (using the pressure impulse data from Table 1). Figure 7 also shows the calculated pressures, assuming $\rho_0 = 350$ kg/m$^3$ and $\rho_f = 500$ kg/m$^3$, as a function of $d_{LC}$ for shock propagation depths into the snow of 0.06, 0.1, 0.2 and 0.3 m. It is evident that air-blast shock pressures, for a given penetration depth into the snow, do not attenuate the same amount for a given shock penetration depth at the different $d_{LC}$. Shock attenuation (that is, pressure reduction after a given shock propagation depth) is greatest near the line charge ($d_{LC} = 0.96$ m) and least at the farthest distance ($d_{LC} = 23.97$ m). This occurs because the duration of the applied air-blast pressure impulse (positive phase duration) increases with $d_{LC}$ (Table 1). The increasing positive phase duration allows the shock to propagate through a greater depth of snow before starting the $\varepsilon^{-2}$ decay. These findings suggest that, for shallow shock penetration depth into a snow cover, line charge pressure reduction depends on the positive phase duration in addition to the total pressure impulse. Also, shock pressure attenuation in a snow cover can be overcome, somewhat, by increasing the positive phase duration of a given pressure impulse.

**Table 1. Air-blast measurements—shot 2 (after Ford 1986).**

| *Distance from line charge (m)* | *Positive phase duration (ms)* | *Peak air-blast pressure (MPa)* | *Peak impulse (kPa s)* |
|---|---|---|---|
| 0.96 | 1.6 | 3.4 | 0.61 |
| 2.99 | 11.0 | 1.64 | 1.36 |
| 6.97 | 16.0 | 0.36 | 0.76 |
| 11.00 | 18.0 | 0.16 | 0.61 |
| 23.97 | 29.2 | 0.07 | 0.60 |

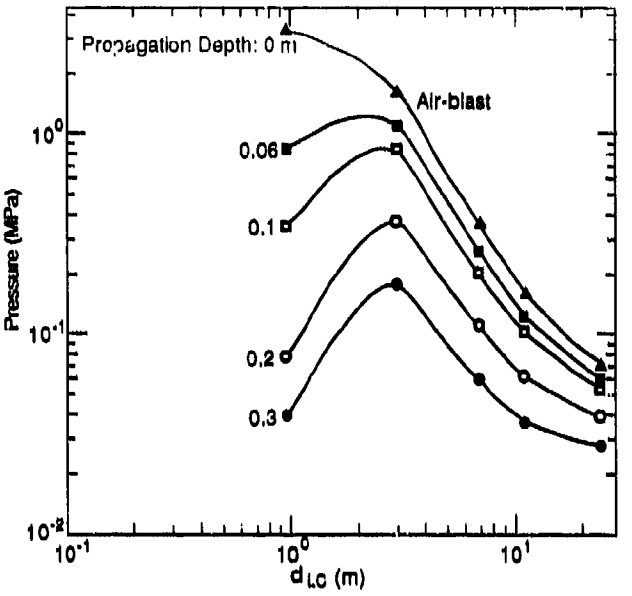


*Figure 7. Pressure decay with distance from the line charge for different shock propagation depths into the snow, predicted by the snowplow model. The air-blast curve is drawn from data given in Table 1.*

## DISCUSSION AND CONCLUSIONS

The snowplow model has a limited ability to describe shock propagation and attenuation in snow because of the simplifying underlying assumptions. The model is, however, capable of giving conservative estimates of shock attenuation in snow and of illustrating some of the important features. Actual shock pressure attenuation will be less than that predicted by the snowplow model using only one compaction step to the final snow density. Better estimates of shock pressure attenuation in snow may be possible using the snowplow model and a more reasonable compaction path for snow.

The snowplow model predicts that snow can cause shock pressures to decay as a function of $X_f^{-2}$ for plane waves, $R^{-4}$ for cylindrical waves and $R^{-6}$ for spherical waves. Brown's (1980) pressure decay estimate of about $X_f^{-1.2}$ for plane waves is different from the decay predicted by the snowplow model. Agreement between the snowplow calculations and Brown's estimates might improve if a realistic snow compaction model were used in the snowplow model.

Mellor (1977) estimates that spherical geometry shocks, where $R >> R_0$, attenuate as $R^{-3}$ to $R^{-4}$ as compared to the snowplow model prediction of $R^{-6}$. It may be that the snowplow model predictions are grossly off because of the simple snow compaction path used in the model or that the field measurements used by Mellor to make his estimates are not the result of shock propagation in snow. The pressure sensors used in many of the field tests were not able to survive near source pressures and were, consequently, located well outside the zone of extreme shock induced snow compaction. Outside the zone of snow compaction, pressure decay is due to viscous dissipation and geometric spreading, which produce much less pressure attenuation than the pore collapse mechanisms described by the snowplow model.

This implies that Mellor's estimates of pressure decay in snow for spherical shocks may be too low, but a final conclusion is not possible until better snow compaction paths are used in the model calculations.

Estimating shock attenuation requires some thoughtful application of the results of this study. Explosive-induced shocks in snow often result from an explosive charge detonation on the snow or in the air above the snow. In this situation the shock will be transmitted into the snow by an air-blast wave propagating over the snow surface. If the initial radius for the air-blast pressure wave striking the snow is assumed to be the distance from the charge source to the position at which the pressure is transmitted into the snow, then in most cases $R_0$ will be much greater than the snow depth (i.e., $\varepsilon << R_0$). Attenuation from the transmission position through the snow will proceed as $\varepsilon^{-2}$ rather than as $R^{-6}$ for spherical waves or $R^{-4}$ for cylindrical waves.

Pressure decay of shock waves in snow can be delayed by increasing the positive phase duration of the applied pressure impulse.

## LITERATURE CITED


**Brown, R.L.** (1980) An analysis of non-steady plastic shock waves in snow. *Journal of Glaciology*, **25**(92): 279–287.

**Brown, R.L.** (1981) A method for evaluating shockwave propagation in snow. *Cold Regions Science and Technology*, **5**: 151–156.

**Brown, R.L.** (1983) A comparison of unsteady wave propagation for various snowpack properties. *Annals of Glaciology*, **4**: 30–36.

**Ford, M.B.** (1986) Mine-clearing performance of XM268 blasting agent line charge. USA Waterways Experiment Station, TR SL-86-4.

**Herrmann, W.** (1971) Constitutive equations for compaction of porous materials. Sandia Laboratories Report SC-DC-71 4134.

**Kolsky, H.** (1963) *Stress Waves in Solids*. New York: Dover Pub., Inc. (republication of work from Clarendon Press, Oxford, 1953).

**Mellor, M.** (1977) Engineering properties of snow. *Journal of Glaciology*, **19**(81): 15–66.

**Torvik, P.J.** (1971) On the attenuation of diverging shock waves. U.S. Air Force Institute of Technology Report AFIT TR 71–4.

# REPORT DOCUMENTATION PAGE

Form Approved
OMB No. 0704-0188

Public reporting burden for this collection of information is estimated to average 1 hour per response, including the time for reviewing instructions, searching existing data sources, gathering and maintaining the data needed, and completing and reviewing the collection of information. Send comments regarding this burden estimate or any other aspect of this collection of information, including suggestion for reducing this burden, to Washington Headquarters Services, Directorate for Information Operations and Reports, 1215 Jefferson Davis Highway, Suite 1204, Arlington, VA 22202-4302, and to the Office of Management and Budget, Paperwork Reduction Project (0704-0188), Washington, DC 20503.

| 1. AGENCY USE ONLY (Leave blank) | 2. REPORT DATE | 3. REPORT TYPE AND DATES COVERED |
|---|---|---|
| | October 1990 | |

**4. TITLE AND SUBTITLE**

Estimates of Shock Wave Attenuation in Snow

**5. FUNDING NUMBERS**

PE: 6.27.84A
PR: 4A762784AT42
TA: CS
WU: 012

**6. AUTHORS**

Jerome B. Johnson

**7. PERFORMING ORGANIZATION NAME(S) AND ADDRESS(ES)**

U.S. Army Cold Regions Research and Engineering Laboratory
72 Lyme Road
Hanover, New Hampshire 03755-1290

**8. PERFORMING ORGANIZATION REPORT NUMBER**

CRREL Report 90-8

**9. SPONSORING/MONITORING AGENCY NAME(S) AND ADDRESS(ES)**

Office of the Chief of Engineers
Washington, D.C. 20314-1000

**10. SPONSORING/MONITORING AGENCY REPORT NUMBER**

**11. SUPPLEMENTARY NOTES**

**12a. DISTRIBUTION/AVAILABILITY STATEMENT**

Approved for public release; distribution is unlimited.

Available from NTIS, Springfield, Virginia 22161

**12b. DISTRIBUTION CODE**

**13. ABSTRACT** (*Maximum 200 words*)

A simple momentum model, assuming that snow compacts to its final density at negligible stress, is used to estimate shock wave attenuation in snow. Four shock loading situations are examined: a one-dimensional pressure impulse of finite duration and instantaneously applied pressure impulses for one-dimensional, cylindrical and spherical shock geometries. Calculations show that while a finite-duration impulse is being applied, the shock pressure in snow is determined by the impulse pressure–time profile. After the pressure impulse has been applied, the one-dimensional shock pressure decay is the same as for an instantaneously applied pressure impulse and is proportional to the inverse square of the shock propagation distance, $(X_f - X_0)^{-2}$. Hence, finite-duration pressure impulses delay the onset of shock attenuation in snow. This can result in more pressure attenuation near a shock source, where the positive phase duration of the shock is short, compared to shock waves farther from a source. Cylindrical waves have a maximum decay that is proportional to the inverse of the propagation radius to the fourth power, $R^{-4}$, and spherical waves have a maximum decay that is proportional to $R^{-6}$. Amplitude decay for cylindrical and spherical shock waves can vary from $(R-R_0)^{-2}$, when $(R-R_0) << R_0$ (where $R_0$ is the interior radius over which a pressure impulse per unit area is applied), to their maximum decay.

**14. SUBJECT TERMS**

Pressure attenuation
Shock waves
Snow
Snow plow model

**15. NUMBER OF PAGES**

20

**16. PRICE CODE**

| 17. SECURITY CLASSIFICATION OF REPORT | 18. SECURITY CLASSIFICATION OF THIS PAGE | 19. SECURITY CLASSIFICATION OF ABSTRACT | 20. LIMITATION OF ABSTRACT |
|---|---|---|---|
| UNCLASSIFIED | UNCLASSIFIED | UNCLASSIFIED | UL |

NSN 7540-01-280-5500

☆ U. S. GOVERNMENT PRINTING OFFICE: 1990—500-061—22045

Standard Form 298 (Rev. 2-89)
Prescribed by ANSI Std. Z39-18
298-102